Literature Survey

Application of Image Restoration Techniques in Flow Scalar Imaging Experiments

Guanghua Wang

Center for Aeromechanics Research

Department of Aerospace Engineering and Engineering Mechanics

The University of Texas at Austin

Austin, Texas 78712-1085

Abstract

Scalar imaging techniques are widely used in fluid mechanics, but the effects of imaging system blur on the measured scalar gradients are often inadequately quantified. Imaging system blur or Point Spread Function (PSF) is very difficult to measure directly and accurately, which prevents the consideration of the blurring effects in flow imaging experiments. For flow scalar images with Poisson noise, Richardson-Lucy Expectation Maximization (R-L-EM) algorithm and Maximum Likelihood (ML) blind deconvolution technique are used to improve the resolution and flow scalar measurement accuracy. Proper constraints and PSF accuracy are very important for the R-L-EM algorithm. ML blind deconvolution is more proper for unknown PSF or PSF is not well measured.

1. Introduction

The spatial resolution of the optical system is very important for flow imaging experiments and it depends on many factors [1], i.e. pixel size of the detector array, depth of the collection optics and magnification etc. In many scalar imaging experiments, the resolution is usually quoted in terms of the area that each pixel images in the flow. For ideal optical system or for optical system used at high f# (f# = f/D, where f is the focal length and D is the diameter of the lens) and magnification is close to the design condition, resolution is nearly diffraction limited. However for low light level flow imaging experiments, like Raman, Rayleigh and Planar Laser Induced Fluorescence (PLIF) imaging, fast (low f#) optics are commonly used. A typical dissipation field from acetone PLIF experimental data [2] is shown in figure 1. For these experiments, pixel size is not the only factor that limits the resolution and the Point Spread Function (PSF) of the imaging system should also be considered, since the image is the convolution of the PSF with the irradiance distribution of the object. The smallest objects that can be resolved are related to the size and shape of the PSF. PSF also tends to progressively blur increasingly smaller structures. This is essentially a result of the system's inability to transfer contrast variations in the object to the image.

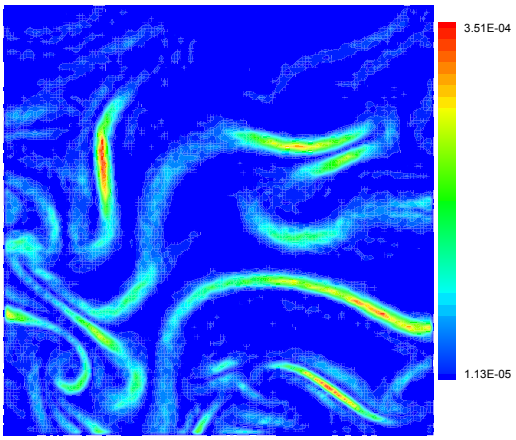

Fig. 1 Dissipation field of an acetone PLIF image [2]

Depending on the flow condition and imaging system, the PSF could be of the same order as the characteristic length scale of the scalar structures in the flow field, which may causes huge error in the scalar measurement. To represent the TRUE scalar structure statistics, i.e. thickness, dissipation rate and Probability Density Function (PDF), it is necessary to restore the experimental images.

2. Background

The general model [3-9] for a linear degradation caused by blurring and additive noise is

$$i = h * o + n \tag{1}$$

where ***i*** is the blurred and noisy image corresponding to the observation of the "true image" ***o***, ***h*** is the blurring function or PSF of the system, ******* is the convolution operator, ***n*** denotes the additive noise, i.e. electronic or quantization noise involved in obtaining the image. In Fourier domain, the degradation is

$$I = H \cdot O + N \tag{2}$$

where ***I***, ***H***, ***O*** and ***N*** are the Fourier transforms of ***i***, ***h***, ***o*** and ***n*** respectively.

The purpose of restoration is to determine ***o*** knowing ***i*** and ***p***. This inverse problem has led to a large amount of work. Main difficulties are coming from the additive noise [3-9] and the PSF [7-9]. The modeling of blurring can be divided in two parts: blurring function ***h*** (PSF) and noise modeling. Some ideal PSF models are Gaussian, out-of-focus and linear motion blur [3]. In astronomy, data extracted from clear stars in observed image is used to fit a synthetic PSF function by weighted nonlinear least squares method [7, 8]. The PSF measurement techniques are also discussed in [1].

The diversity of algorithms [3-9] developed nowadays reflects different ways of recovering a "best" estimate of the "true image". Wiener and regularized filters are better for known PSF and additive noise [3, 4]. Some iterative restoration techniques [10], i.e. Expectation Maximization (EM) algorithms, work better for known PSF and unknown additive noise. Blind image restoration algorithms [5, 6] are more proper for unknown PSF and additive noise. Flow imaging experiments have a lot in common with astronomy observations. They are both low light level imaging. Both images are degraded by imaging optical system and suffer from signal related noise (Poisson noise), CCD camera read-out noise and quantization noise etc. These physical similarities suggest that a better starting point in applying image restoration techniques in flow scalar image restoration is to consider those successful ones in astronomy.

3. Richardson-Lucy Expectation Maximization (R-L-EM) algorithm

The Richardson-Lucy algorithm ([11, 12]), also called the expectation maximization (EM) method, is an iterative technique used heavily for the restoration of astronomical images in the presence of Poisson noise [7-9]. It attempts to maximize the likelihood of the restored image by using the Expectation Maximization (EM) algorithm [10]. The EM approach consists of constructing the conditional probability density [7, 10]

$$p(o \mid i) = p(i \mid o)\, p(o) / p(i) \tag{3}$$

where $p(i)$ and $p(o)$ are the probabilities of the observed image ***i*** and the true image ***o***. $p(i \mid o)$ is the probability distribution of observed image ***i*** if ***o*** were the true image. The Maximum Likelihood (ML) solution maximizes the density $p(i \mid o)$ over o :

$$o_{ML} = \arg\max_{o} p(i \mid o) \tag{4}$$

where "argmax" means "the value that maximizes the function". For true image ***o*** with Poisson noise, the probability $p(i \mid o)$ is:

$$p(i \mid o) = \prod_{x,y} e^{-(h*o)} \frac{(h*o)^{i}}{i!} \tag{5}$$

The maximum can be computed by taking the derivative of the logarithm $\partial \ln p(i \mid o) / \partial o = 0$. The EM algorithm consists of two steps [11]: expectation step (E-step) and maximization step (M-step). These two steps are iterated until converging. In practice, they are usually combined together to save the storage of results from E-step. Assuming the PSF is normalized to unity, a typical iteration is:

$$o^{(k+1)} = o^{(k)} \left[h^{*} * \frac{i}{h * o^{(k)}} \right] \tag{6}$$

where $h^{*}(x, y) = h(-x, -y)$, h^{*} is the transpose of the PSF, and $o^{(k)}$ is the estimate of the true image ***o*** after ***k*** iterations. The image $h * o^{(k)}$ is referred to as the re-blurred image [13]. Eqn. (6) is the basic iteration step of R-L-EM algorithm and it converges to the ML solution for Poisson statistics in the data. Constraints, i.e. non-negativity (i.e., estimate of the image must be positive), finite support (i.e., the object belongs to a given spatial domain), band-limited (i.e., the Fourier transform of the object belongs to a given frequency domain) and local and global conservation of flux at each iteration, can be incorporated easily in the basic iterative scheme.

Every iteration of the EM algorithm increases the likelihood function until a point of (local) maximum is reached. When the number of iterations increases, the iteration first approaches the unknown object and then potentially goes away from it. One way to suppress the noise amplification with increasing iterations is to use the following iterative scheme:

$$o^{(k+1)} = f\left\{o^{(k)}\left[h^{*} * \frac{i}{h * o^{(k)}}\right]\right\} \tag{7}$$

where $\boldsymbol{f}$ is the projection operator that enforces the set of constraints on $o^{(k)}$ and some forms of $\boldsymbol{f}$ are given in [7-9]. The stopping rule is often based on the statistics of residual noise or to employ noise attenuation methods. There are many modifications and improvements to overcome different drawbacks in the original R-L-EM algorithm, i.e. noise handling [7-9] and iteration acceleration [13].

4. Maximum Likelihood (ML) Blind Deconvolution algorithm

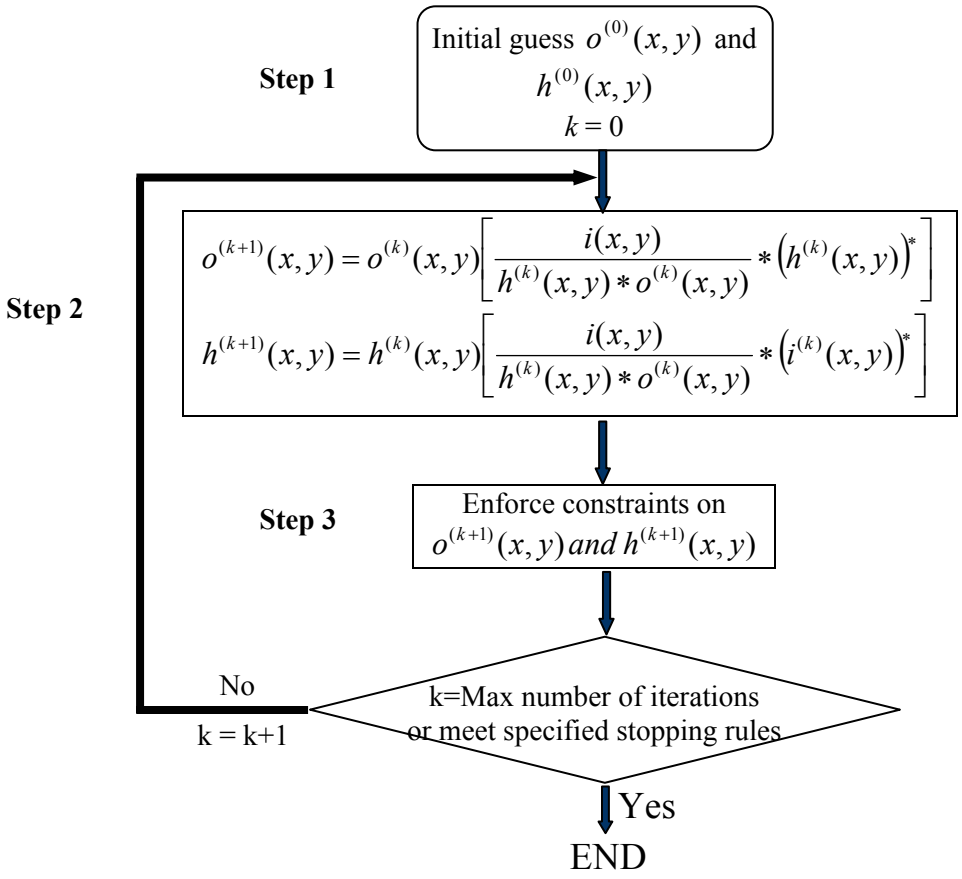

Fig. 2 General flow chart of the ML blind deconvolution algorithm [14]: $o^{(k)}$ is the estimate of the true image of the k-th iteration, $h^{(k)}$ is the restored PSF of the k-th iteration, $(\cdot)^{*}$ is the transpose operator

Blind image deconvolution techniques are systematically reviewed in [4-5] which are more proper when the PSF and noises in the image are both unknown. The general ML blind deconvolution algorithm is summarized in figure 2 [14]. In step 1, initial guesses of the true image $\boldsymbol{o^{(0)}(x, y)}$ and the PSF $\boldsymbol{h^{(0)}(x, y)}$ are made. Step 2 is designed from the optimization strategy specified by the EM algorithm which is similar to Eqn. (6). Step3 enforces reasonable constrains on the solutions of the restored image and PSF

which is important to make unambiguous blind deconvolution possible. This algorithm also needs a quantitative criterion for stopping the iteration. Same rules as those in R-L-EM algorithm can be used and simple rules based on number of iterations were also used [14]. The PSF estimate may not be unique. By making additional assumptions on the symmetry, sign, support and/or scaling of the PSF, a unique solution may be obtained. Some constraints on PSF are shown in table 1 [14].

Constraint	**Formula**
Unit summation	$h^{(k+1)}(x,y) = h^{(k+1)}(x,y) \Big/ \sum_{x,y} h^{(k+1)}(x,y)$
Finite spatial support	For all of (x, y) outside some region, $h^{(k+1)}(x,y) = 0$
Band-limited	$H^{(k+1)}(u,v) = FFT\left(h^{(k+1)}(x,y)\right)$, For all of (u, v) outside some region, $H^{(k+1)}(u,v) = 0$
Non-negativity	$h^{(k+1)}(x,y) = FFT^{-1}\left(H^{(k+1)}(u,v)\right)$, For all (x,y): if $h^{(k+1)}(x,y) < 0$, then $h^{(k+1)}(x,y) = 10^{-30}$

Table 1 Summary of constraints on the PSF [14]

The main advantage of this technique is that no parametric form of the PSF is required and the algorithm has low computational complexity. The complexity of the algorithm is $O(N_i)$, where N_i is the number of pixels in the true image. This algorithm allows one to obtain explicit equations for the blur, noise, and power spectra. The main disadvantage is that the iteration might converge to a local maximum. Multi-channel extension of the algorithm has been developed and showed more reliable restoration [7].

5. Complexity and Simulation

The R-L algorithm has the general form of an iterative formula in which the value of a pixel at each iteration is equal to the previous one multiplied by a modifying factor (Eqn. 6). In order to enforce constraints (Eqn. 7), the projection and back-projection operations can be performed using the fast Fourier transform (FFT). Each iteration needs one FFTs in the projection step and one in the back-projection step depending on how many constrains are applied. All other computations are vector operations that have little impact on CPU time. Thus the R-L-EM algorithm is basically an algorithm with two FFTs per iteration. Typical R-L EM restoration results are shown in figure 3 and 4 [8].

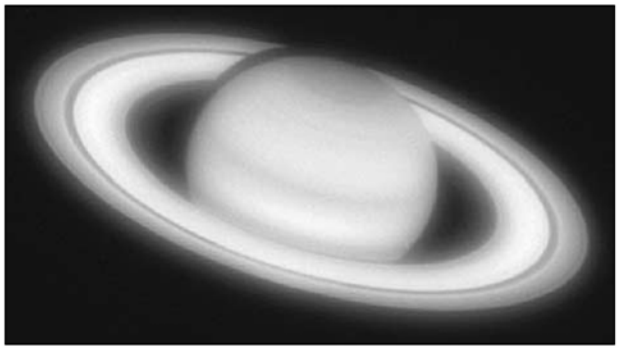

Fig. 3 Raw image of planet Saturn from Hubble Space Telescope (Fig. 8 in [8])

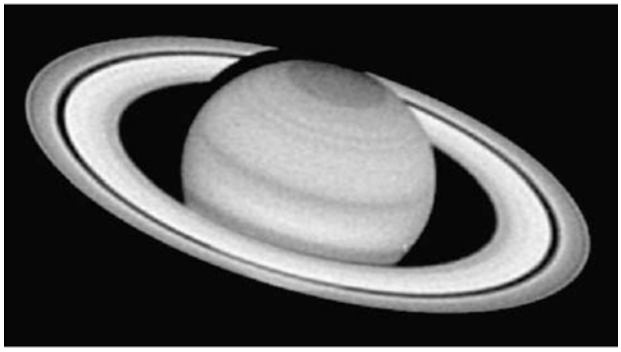

Fig. 4 Reconstruction of the image of Saturn using the R-L algorithm (Fig. 9 in [8])

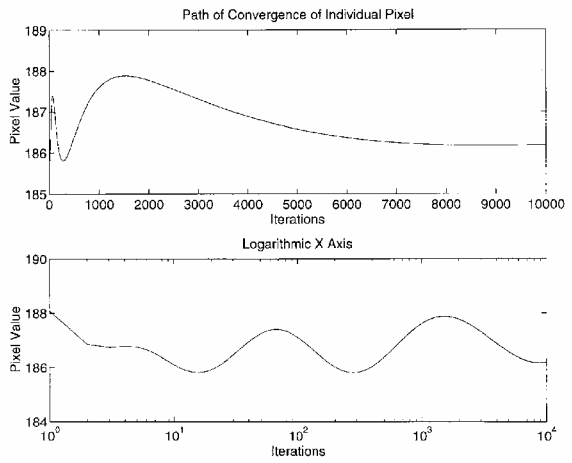

Fig. 5 Path of an individual pixel over 10,000 R-L-EM iterations in linear (top) and logarithmic scales (bottom) (Fig. 1 in [13])

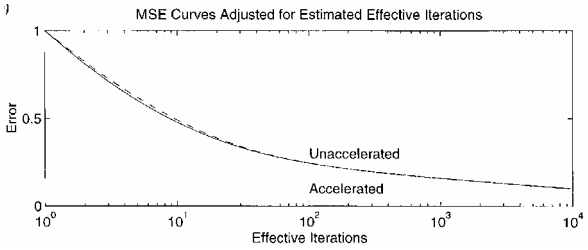

Fig. 6 Mean Square Error (MSE) between original and restored image plotted with effective iterations; Un-accelerated (10,000 iterations, solid curve); accelerated (250 iterations, dashed curve) (Fig. 6(b) in [13])

An individual pixel normally changes most rapidly in the first few iterations and slower as the restoration continues. Figure 5 shows the path of an individual pixel from a 10,000-iteration R-L-EM restoration on an 8-bit image [13]. In the logarithmic scale, it shows that the characteristic scale of the oscillations increases exponentially. A new method, called Automatic Acceleration [13], has been developed to achieve significantly increased acceleration with little computational overhead. An example R-L-EM restoration achieves an average speedup of 40 times after 250 iterations as shown in figure 6.

From the point of view of the computation requirements for ML blind deconvolution algorithm, the number of FFTs in each iteration will de doubled comparing to that of the R-L-EM algorithm due to the additional constraints on the estimate of the PSF. The restored image and PSF from ML blind deconvolution algorithm are shown in figure 7 and 8 [14] respectively. Simulation results also show that there is a trade-off between the sharpness of the true image estimate and noise amplification. The

estimation of the noise variance is usually smaller than that given by a true Wiener filter [7]. It has also been found that the proper incorporation of constraints improves image restoration significantly [14].

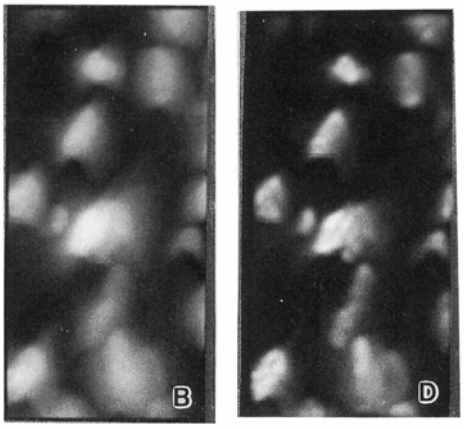

Fig. 7 (B) is the side view of the original biological image; (D) is the restored image by ML blind deconvolution after 600 iterations (Fig. 9 in [14])

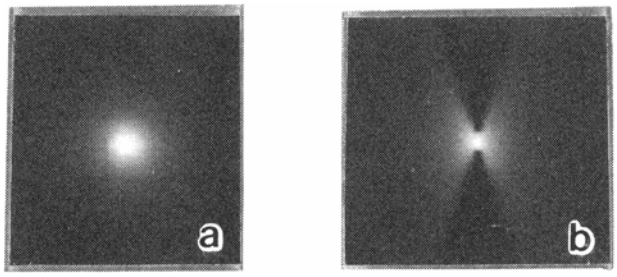

Fig. 8 Summed intensity projections of the PSF reconstructed from the same data as that of figure 7 after 600 iterations. (a) top projection; (b) side projection (Fig. 10 in [14])

6. Conclusion

The most successful algorithms are those most cognizant of the physical constraints on the image, PSF and noise. Similar underlying physical properties between flow scalar imaging experiments and astronomy observations suggest that most of the successful algorithms in astronomy image restoration can be applied in flow scalar image restoration. For most flow scalar imaging experiments, sequence short exposure of scalar images is usually recorded and multi-channel restoration technique may be used to get more reliable restorations [15]. Multi-scale restoration techniques are also developed to restore astronomy observation images, i.e. wavelet-Lucy algorithm [7]. The underlying physical implication is very close to the scalar cascade hypothesis in fluid mechanics which may deserve further studying.

Although most image restoration algorithms were successfully used in astronomy and biology, no applications of these algorithms were found in the restoration of flow scalar images. One reason (I thought) is that many forms of deconvolution algorithms are too mysterious and needs going through a lot to understand them. The other is probably that most flow imaging techniques are relatively young (i.e. PLIF is about 10 years old) and most researches are involving in different applications instead of refining. This project will introduce image restoration techniques in flow scalar imaging applications and focus on how scalar measurements are improved by these methods.

Reference

1. N. T., Clemens, “Flow Imaging”, in “Encyclopedia of Imaging Science and Technology”, Editor: J.P. Hornak, John Wiley and Sons, New York, 2002
2. M. S. Tsurikov and N. T. Clemens, “The structure of dissipative scales in axisymmetric turbulent gas-phase jets”, AIAA Paper 2002-0164, AIAA 40th Aerospace Sciences Meeting, 2002
3. R. L. Lagendijk and J. Biemond, “Basic Methods for Image restoration and Identification”, in “Handbook of image and video processing”, Editor: Al Bovik, Academic Press, San Diego, 2000
4. V. M. R. Banham and A. K. Katsaggelos, “Digital Image Restoration”, IEEE Signal Processing Magazine, vol. 14, no. 2, pp. 24-41, Mar.1997
5. T. D. Kundur and D. Hatzinakos, “Blind Image Deconvolution”, IEEE Signal Processing Magazine, vol. 13, no. 3, pp. 43-64, May 1996
6. T. D. Kundur and D. Hatzinakos, “Blind Image Deconvolution Revisted”, IEEE Signal Processing Magazine, vol. 13, no. 6, pp. 61-63, Nov. 1996
7. J. Starck, E. Pantin and F. Murtagh, “Deconvolution in Astronomy: A Review”, Publications of the Astronomical Society of the Pacific, vol. 114, pp. 1051-1069, Oct. 2002
8. R. Molina, J. Nunez, F. J. Cortijo and J. Mateos, “Image Restoration in Astronomy: A Bayesian Perspective”, IEEE Signal Processing Magazine, vol. 18, no. 2, pp.11-29, Mar. 2001
9. R. J. Hanisch, R. L. White and R. L. Gilliland, “Deconvolutions of Hubble Space Telescope Images and Spectra”, in “Deconvolution of Images and Spectra”, Editor: P.A. Jansson, 2nd ed., Academic Press, CA, 1997
10. T.K. Moon, “The Expectation-Maximization algorithm”, IEEE Signal Processing Magazine, vol.13, no.6, pp.47-60, Nov. 1996
11. W. H. Richardson, “Bayesian-based iterative method of image restoration”, J. Opt. Soc. Amer., vol. 62, pp. 55-59, 1972
12. L. B. Lucy, “An iterative technique for the rectification of observed distribution”, Astron. J., vol. 79, pp. 745-754, 1974
13. D.S.C., Biggs and M., Andrews, “Acceleration of iterative image restoration algorithms”, Applied Optics, vol. 36, no. 8, pp1766-1775, 1997
14. T.J. Holmes, S. Bhattacharyya, J.C. Cooper, D.H. Hanzel, V. Krishnamurthi, W-C. L., B. Roysam, D.H. Szarowski and J.N. Turner, "Light Microscopic Images Reconstructed by Maximum Likelihood Deconvolution", in "Handbook of Biological Confocal Microscopy", Editor: J. B. Pawley, Plenum Press, New York, 1995
15. X. H.-T. Pai, A. C. Bovik, and B. L. Evans, "Multi-Channel Blind Image Restoration", TUBITAK Elektrik Journal of Electrical Engineering and Computer Sciences, vol. 5, no. 1, pp. 79-97, Fall 1997